



Dalton
Transactions

**Ligand Effects on Electronic Structure and Bonding in U(III)
Coordination Complexes: A Combined MCD, EPR and
Computational Study**

Journal:	<i>Dalton Transactions</i>
Manuscript ID	DT-ART-08-2020-002929.R1
Article Type:	Paper
Date Submitted by the Author:	18-Aug-2020
Complete List of Authors:	Wolford, Nikki; University of Rochester YU, Xiaojuan; University at Buffalo, State University of New York Bart, Suzanne; Purdue University Autschbach, Jochen; University at Buffalo, State University of New York, Chemistry Neidig, Michael; University of Rochester

SCHOLARONE™
Manuscripts

ARTICLE

Ligand Effects on Electronic Structure and Bonding in U(III) Coordination Complexes: A Combined MCD, EPR and Computational Study

Received 00th January 20xx,
Accepted 00th January 20xx

DOI: 10.1039/x0xx00000x

Nikki J. Wolford^{a†}, Xiaojuan Yu^{b†}, Suzanne C. Bart^c, Jochen Autschbach^{b*}, Michael L. Neidig^{a*}

The trivalent oxidation state of uranium has been shown to undergo unique reactivity, from its ability to activate a variety of small molecules to its role in the catalytic reduction of ethene to ethane amongst others. Central to this unique reactivity and ability to rationally design ligands for isotope separation is the underlying uranium electronic structure. While electronic structure studies of U(IV), U(V), and U(VI) have been extensive, by comparison, analogous studies of more reduced oxidation states such as U(III) remain underdeveloped. Herein we report a combined MCD and EPR spectroscopic approach along with density functional theory and multireference wavefunction calculations to elucidate the effects of ligand perturbation in three uranium(III) Tp* complexes. Overall, the experimental and computational insight suggests that the change in ligand environment across this series of U(III) complexes resulted in only minor perturbations in the uranium electronic structure. This combined approach was also used to redefine the electronic ground state of a U(III) complex with a redox non-innocent Bipy⁻ ligand. Overall, these studies demonstrate the efficacy of the combined experimental and theoretical approach towards evaluating electronic structure and bonding in U(III) complexes and provide important insight into the challenges in altering ligand environments to modify bonding and reactivity in uranium coordination chemistry.

Introduction

Uranium coordination chemistry has been an area of broad research interest, motivated by applications ranging from ligand design for chemical separations of spent nuclear fuel waste¹ to reactivity in areas such as small molecule activation.^{2,3} Central to understanding the reactivity and bonding is the underlying electronic structure of the coordination complexes as a function of oxidation state, coordination number and geometry, and ligand architecture. As such, there has been tremendous effort towards developing fundamental insight into the electronic structure and bonding in uranium chemistry to rationalize the reactivity observed experimentally. These studies have utilized computational data combined with a variety of spectroscopic techniques including NMR, electron paramagnetic resonance (EPR), electronic absorption (EAS), magnetic circular dichroism (MCD), extended X-ray absorption fine structure (EXAFS), and X-ray absorption near-edge structure (XANES) spectroscopies as well as SQUID magnetometry.⁴⁻¹⁸

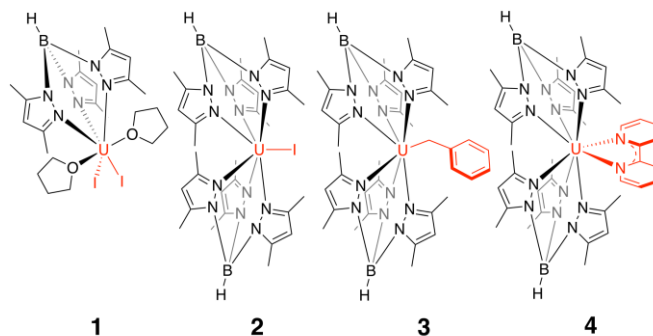


Figure 1: Structures of Tp*UCl₂ (1), Tp*₂UI (2), Tp*₂UBn (3), and Tp*₂UBipy (4).

While utilization of these techniques has resulted in copious studies which provided insight into the electronic structures of coordination complexes of the U(VI), U(V), and U(IV) oxidation states, insight into more reduced uranium oxidation states, such as U(III), remain significantly underdeveloped. While electronic absorption spectroscopy can provide insight into the electronic structure in f-element systems, due to the Laporte forbidden nature of d-d and f-f transitions, traditional absorption spectra in the NIR region suffer from very weak signal intensity as well as the potential for vibrational overtones arising from solvent. In the UV-visible region, overlapping transitions often result in broadened spectral features which can be difficult to assign. In addition, low temperature absorption techniques often require specialized setups to obtain spectroscopic data which would still suffer from low signal intensity. By contrast, MCD spectroscopy

^a Department of Chemistry, University of Rochester, Rochester, New York 14627, USA. *Email: neidig@chem.rochester.edu

^b Department of Chemistry, University at Buffalo, State University of New York, Buffalo, New York 14260, USA. *Email: jochena@buffalo.edu

^c H.C. Brown Laboratory, Department of Chemistry, Purdue University, West Lafayette, Indiana 47907, USA.

† Nikki J. Wolford and Xiaojuan Yu contributed equally to this work.

Electronic Supplementary Information (ESI) available: [details of any supplementary information available should be included here]. See DOI: 10.1039/x0xx00000x

provides improved spectral resolution, the possibility for positive and negative features which allow for separation of broadened signals, as well as the ability to observe the formally forbidden f-f and d-d transitions.

MCD spectra can result from three different terms, *A*-, *B*- and *C*-terms. *A*- and *B*-term transitions are temperature independent and arise from the Zeeman splitting of the excited state and field induced mixing of zero-field states, respectively. *C*-term MCD transitions are temperature and field dependent and arise from the removal of ground state degeneracy in the presence of a magnetic field. These transitions are particularly sensitive to changes in the electronic structure in paramagnetic centers which have large spin-orbit coupling constants, such as actinides. Perhaps most importantly, *C*-term MCD is extremely sensitive to the orbital location of unpaired electrons, which results in drastic changes in spectral features when oxidation or spin state changes occur. The paramagnetic nature and Kramers ground state of the U(III) oxidation state makes it an ideal candidate for electronic structure studies using the combination of *C*-term MCD and EPR spectroscopy.

Towards this, the availability of a series of molecules with minor perturbations in ligand environment allow for a systematic study in the effect of ligand type on the U(III) oxidation state. In 2012, Bart and coworkers reported a U(III) tris(3,5-dimethyl-1-pyrazolyl)borate (Tp*) alkyl complex, Tp*₂UBn, which could functionalize CO₂ and CS₂ via an insertion reaction, resulting in the formation of the uranium dicarboxylate and dithiocarboxylate complexes.¹⁹ The Tp* ligand scaffold utilized in the isolation of Tp*₂UBn is very robust and simple to synthesize on large scale. Additionally, the chemistry of uranium Tp* complexes have been well established by Takats and co-workers over the last several decades,²⁰⁻²² being expanded upon by Bart and co-workers more recently.^{15, 19, 23, 24}

We sought to utilize the Tp* ligand platform to address this gap in understanding of electronic structure and bonding in such U(III) complexes. Towards this, we utilized electronic absorption (EAS), electron paramagnetic resonance (EPR) and magnetic circular dichroism (MCD) spectroscopies combined with density functional theory (DFT), time-dependent DFT (TD-DFT), and multi-reference wavefunction calculations. In particular, *C*-term MCD spectroscopy has recently been shown to provide tremendous insight into both U(IV) and U(V) complexes,^{16, 18} yet this technique has not been reported for U(III) complexes. Specifically, the studies presented herein apply the aforementioned spectroscopic and theoretical methods to define electronic structure and bonding in a series of U(III) Tp* complexes (Tp*UI₂ (**1**), Tp*₂UI (**2**), and Tp*₂UBn (**3**), Figure 1)^{19, 20, 22} Lastly, this combined approach is shown to be a powerful method in elucidating the electronic structure of a related uranium complex with a redox non-innocent bipyridine (Bipy) ligand, Tp*₂UBipy (**4**) (Figure 1).²³

Results and Discussion

Experimental and Theoretical EPR Spectroscopy of Complexes 1-3

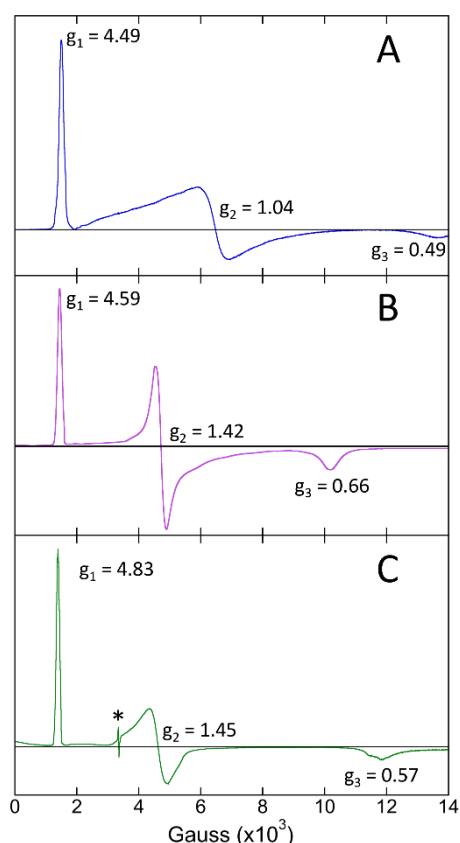


Figure 2: 5 K EPR spectra of solid samples prepared for **1** (A, top, blue), **2** (B, middle, purple) and **3** (C, bottom, green). *radical signal from KBN, $g = 2.002$.

Initial studies into the electronic structure and bonding of the uranium(III) Tp* complexes focused on the effects of ligand perturbation on the EPR spectra across the series of complexes **1-3**. While EPR spectroscopy has been used to characterize U(V) complexes, examples of uranium(III) EPR are limited to just a handful of spectra.^{5, 12, 25-29} In rhombic systems of uranium(III) where one would expect to observe three distinct EPR signals, often only two are experimentally observed due to instrument field range limitations. The third is instead theoretically determined. The capability to scan a wider magnetic field range (0-14000 G) at cryogenic temperatures (5 K) has allowed for the experimental determination of all three *g*-factors in complexes **1-3**.

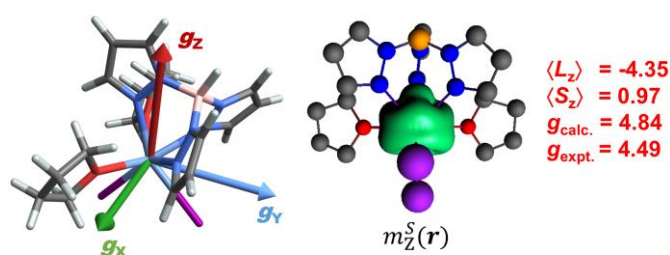


Figure 3: Orientation of the principal magnetic axes of complex **1**, and GS spin magnetization isosurfaces for quantization in the direction of the magnetic Z axis. The isosurface values are ± 0.001 au.

Complex **1** was isolated from the reaction of 1 equivalent of KTp^* with $\text{U}(\text{THF})_4$.²² The solid state 5 K EPR spectrum of **1** exhibits a highly rhombic series of transitions with $g_1 = 4.49$, $g_2 = 1.04$, and $g_3 = 0.49$ (Figure 2A, blue). The reaction of **1** with an additional equivalent of KTp^* results in the formation of complex **2**.²⁰ The solid state 5 K EPR spectrum of **2** also exhibits a rhombic signal but with observed shifts in all three g -factors to lower field, where $g_1 = 4.59$, $g_2 = 1.42$, and $g_3 = 0.66$ (Figure 2B, purple). Reaction of **2** with 1 equivalent of benzylpotassium results in the formation of complex **3**.¹⁹ The 5 K EPR spectrum of **3** is also rhombic, with $g_1 = 4.83$, $g_2 = 1.45$, and $g_3 = 0.57$ (Figure 2C). The g_1 and g_2 values are similar to those previously reported for uranium(III) complexes, and the g_3 values are similar to the previously calculated values (Table S5).

To understand the origin of the experimentally observed transitions, the electronic structures of **1-3** were further investigated using relativistic all-electron complete active space (CAS) multireference wavefunction theory, including spin-orbit (SO) coupling, as implemented in OpenMolcas.^{30, 31} Complete computational details for these calculations as well as for the density functional calculations discussed later, are given in the Supporting Information. The calculated relative energies at the CAS-SO level between the ground states (GSs) and low-lying excited states (ESs) of these complexes are listed in Table S1. The GSs are Kramers doublets, with about 87 to 89% weight from states with U^{3+} ground term (^4I) parentage, and 6 to 8% weight from SO coupling with states deriving from the excited ^2H ion term. The systems feature complex multi-configurational GSs and low-energy excited states. For example, the overall energetic splitting of the $^4\text{I}_{9/2}$ ion level in **1** was calculated to be 613 cm^{-1} , with the first excited state appearing 117 cm^{-1} above the GS.

The calculated largest g -factors of these complexes, in the range of 4.20 to 4.84 at the CAS-SO level, are comparable to the range of 4.49 to 4.83 determined experimentally. The spin and angular momentum expectation values for the principal magnetic axes, and the corresponding g -factors of complexes **1-3**, are provided in Table S2. In all cases, the GS exhibits a large magnetic anisotropy. We focus on **1** as an example representing the similar magnetic properties of complexes **1-3**. The CAS-SO calculation gave $g_x = 0.15$, $g_y = 0.81$ and $g_z = 4.84$ for the GS, in increasing magnitude, with Z labelling the 'easy' magnetic axis and corresponding to g_1 in Figure 2 and the accompanying discussion. The corresponding spin and orbital magnetizations, and natural spin orbitals (NSOs), were generated according to the literature.³²⁻³⁵ The magnetic axes are shown in Figure 3 relative to the molecular frame, along with the spin magnetization. In the absence of SO coupling, the latter would correspond to the usual spin density. For the analysis, the GS component with positive $\langle S_z \rangle$ was selected. A large orbital magnetization $\mathbf{m}_z^L(\mathbf{r})$ with opposite sign to the spin magnetization $\mathbf{m}_z^S(\mathbf{r})$ was calculated. The magnetizations integrate to the expectation values $\langle L_z \rangle = -4.35$ and $\langle S_z \rangle = 0.97$ from which follows $|g_z| = 2|\langle L_z \rangle + g_e \langle S_z \rangle| = 4.84$. Accordingly, the dominant contribution to the electron magnetic moment is from unquenched orbital angular momentum, whereas the contribution from the spin angular momentum is smaller than and of opposite sign to the orbital angular momentum. According to Hund's rules, the spin and orbital angular momentum for an f^3 ion are antiparallel, $J = L - S$, with $L = 6$ and $S = 3/2$. However, due to the combined action of the ligand field and the SO coupling, the spin and orbital angular momentum expectation values calculated for **1** deviate strongly from the largest free ion term projection quantum numbers $M_S = 3/2$ and $M_L = 6$.

The NSOs are the eigenfunctions of the spin magnetization, with populations—each in the range 0 to 1—that add to $2\langle S_z \rangle$. In the

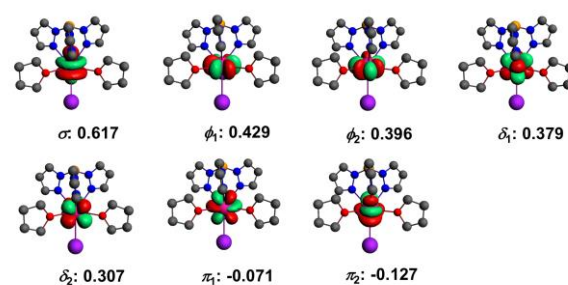


Figure 4: NSOs for the Z direction of the spin magnetization and corresponding spin populations. Ground state component with $\langle S_z \rangle > 0$. The isosurface values are ± 0.03 au.

single-reference scalar relativistic DFT calculations (*vide infra*), there are three unpaired $5f$ spin orbitals, which therefore represent three NSOs with populations of +1 and $\langle S_z \rangle = M_S = 3/2$. The wavefunction calculation shows, however, that the SO GS of **1** is complex, and characterized by five NSOs with important α -spin contributions, along with minor β -spin contributions due to SO coupling (Figure 4). The NSOs can be classified as $5f$ σ , π , δ , ϕ , with the symmetry labels referring to a rotational axis coinciding with the magnetic axis Z. As shown previously for lanthanide complexes³⁵, for f -shell configurations in which two ϕ or two δ (or two π) NSOs have similar spin populations, ideally around 0.5, this is indicative of the presence of orbital angular momentum. Therefore, the NSOs and their occupations indirectly also show that there is a large orbital angular momentum contribution to the magnetic behaviour of the GS of **1**. For completeness, isosurface plots of the orbital magnetization components are shown in Figure S3.

NIR MCD Spectroscopy of Complexes 1-3

To gain further insight into the electronic structure of the $\text{U}(\text{III})$ ion in these complexes, MCD spectroscopy in the near-infrared energy region (NIR) region was utilized. The NIR region of metal-centered coordination complexes often provides information involving metal-based transitions such as f - f or d - d transitions. Unfortunately, these types of metal-based transitions are Laporte forbidden and in traditional electronic absorption spectroscopy are very low in intensity, if observed at all. In contrast, C -term MCD spectroscopy results from the splitting of a magnetically degenerate ground state in the presence of an applied magnetic field due to Zeeman splitting. This results in a non-zero C -term transition if the transitions in question are dipole-allowed, where the intensity is dependent on the magnitude of the spin-orbit coupling constant. Due to this, transitions with significant metal character such as d - d and f - f transitions exhibit increased intensity in C -term MCD relative to electronic absorption compared to light-atom ligand-based charge transfer transitions. The very large spin-orbit coupling constant of actinides make them ideal for studying the f - f transitions in coordination complexes as a function of ligand environment and provide insight into the extent of bonding interactions of the f -orbitals.

Towards this, finely ground powders of complexes **1-3** were used to prepare mull samples for MCD using isopentane (see SI). Spectra were collected as a function of magnetic field and temperature to confirm their C -term origin by both temperature and field dependence (Figures S1/S2). All transitions were observed to be both temperature and field dependent, consistent with C -term behavior. The 5 K, 7 T NIR MCD spectra of complexes **1-3** consist of five

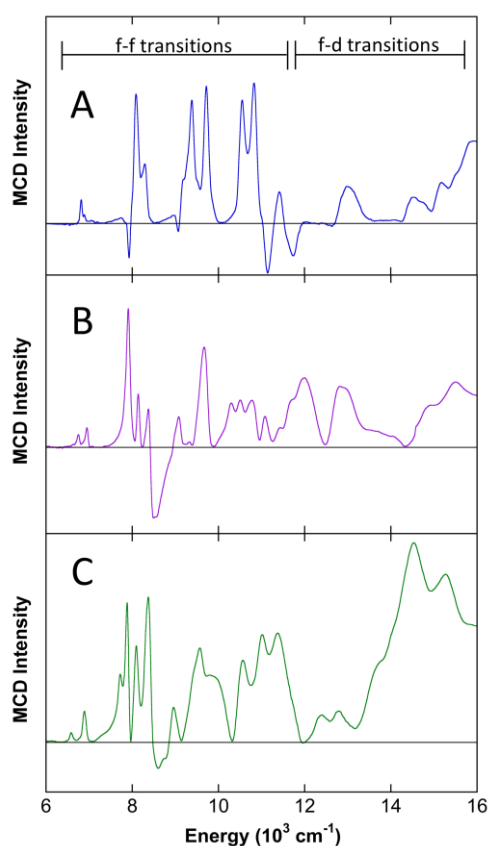


Figure 5: 5 K, 7 T NIR MCD spectra of solid mull samples prepared for **1** (A, top, blue), **2** (B, middle, purple) and **3** (C, bottom, green).

groupings of transitions across the energy region (Figure 5). The first four groupings of transitions, from 6000-13000 cm^{-1} respectively, are very sharp, consistent with previously reported f-f transitions in uranium(III) complexes. From previously reported free-ion calculations performed on trivalent uranium³⁶ as well as calculations performed herein, the ground state of all three complexes is of free-ion level $4f_{7/2}$ parentage. Free-ion calculations of trivalent uranium coordination complexes predict transitions in the energy region of 6000-8000 cm^{-1} which are assigned to f-f transitions from the $4f_{7/2}$ ground state to the $4f_{3/2}$ free-ion state.³⁶ In all three complexes these transitions can be observed. In the energy region of 8000-9000 cm^{-1} , free-ion calculations predict transitions to the $4f_{5/2}$ state³⁶ which are also observed in this energy region of the NIR MCD. The 9000-10000 cm^{-1} energy predicts transitions to the $2H_{7/2}$ state³⁶, which can be observed in complexes **1-3**. The transitions predicted from 8000-10000 cm^{-1} are also assigned as f-f transitions, consistent with the sharp features observed in this energy region of **1-3**.

The last region of assigned f-f transitions observed in these complexes is in the energy region from 10000-12000 cm^{-1} . The free-ion calculations determined these transitions are excitations to the $4f_{5/2}$ and a mixed free-ion state consisting of $4S_{3/2} + 4G_{5/2} + 4F_{7/2} + 4I_{15/2}$ character.³⁶ The higher energy grouping of transitions observed in the NIR MCD of **1-3** (12000-16000 cm^{-1}) can be assigned to f-d transitions (Figure 5). These transitions have undergone significant broadening when compared to the f-f transitions observed at lower energy, consistent with the assignment of f-d transitions. Overall, all three complexes have similar groupings of transitions in the NIR region, especially complexes **2** and **3** which have analogous

geometrical arrangements. This suggests that, as previously observed by our group for U(IV) complexes using MCD spectroscopy, the electronic structure of these complexes is minimally perturbed even with different ligand substitutions, whereas oxidation state and geometry dominate the observed spectral features.

Experimental UV-vis Electronic Absorption Spectroscopy and MCD of Complexes 1-3

While the NIR energy region displays metal-based transitions, the UV-vis energy region displays metal-ligand interactions in the form of ligand-to-metal and metal-to-ligand charge transfer (LMCT/MLCT) transitions. Unlike d-d and f-f transitions, LMCT and MLCT transitions are suppressed in intensity in MCD spectroscopy when compared to traditional EAS due to the decreased metal character of the transitions. This is a very useful consequence, as transitions which are very high in intensity in EAS and decrease in intensity by MCD, are often easily assigned as CT transitions. This combined approach was applied to this series of U(III) complexes where traditional EAS spectra were compared to MCD spectra in the UV-vis region (Figure 6).

In this energy region, there is some energy overlap between the two instruments utilized for obtaining the NIR and UV-vis MCD spectra, respectively. Due to this, the f-d transitions observed in the NIR energy region (Figure 5) can also be observed in the UV-vis spectra of Figure 6. These f-d transitions are Laporte allowed, unlike the f-f and d-d transitions, which results in observation of these transition in the EAS spectra of all three complexes in the energy region of 16000-20000 cm^{-1} . A comparison of the experimental MCD (Figure 6, bottom) and EAS (Figure 6, top) of the energy region of these f-d transitions (16000-20000 cm^{-1}) shows good agreement between the two techniques and also outlines the increased resolution observed in MCD spectroscopy.

The higher energy UV-vis region (> 20000 cm^{-1}) in the EAS spectra have very large intensities, suggestive of CT transitions in these complexes. Further supporting this, the transitions observed by MCD in this energy region are much smaller in intensity, also consistent with CT type transitions. While these preliminary assignments as f-d and CT transitions are consistent with experimental data, further evidence was obtained to provide insight into the exact origin of these transitions and the electronic structure of complexes **1-3**. Due to the highly complex nature of theoretical computations on f^3 complexes, calculations of the MCD spectra were not feasible at present. Instead, DFT/TD-DFT and calculated absorption spectra were used to assign the experimentally observed transitions.

Theoretical Electronic Structure and Electronic Absorption of Complexes 1-3.

For additional insight into the electronic structures of the uranium(III) complexes **1-3**, time-dependent DFT (TD-DFT), natural localized molecular orbital (NLMO)^{37, 38} analyses of the GSs, and natural transition orbital (NTO)³⁹ analyses of the electronic excitations were performed. Canonical molecular orbital (MO) diagrams obtained with DFT are shown in Figure S4. The NLMO and NTO analyses of these complexes are provided in Figure S5 and S8. As already mentioned, in the case of complexes **1-3**, the ground states resulted from three unpaired electrons in quasi-degenerate orbitals and represent $M_S = 3/2$ spin quartet components.

The absorption spectrum of complex **1** can be assigned to at least 4 transitions across the energy region of 12000-30000 cm^{-1} (Figure 6, top left). Based on the TDDFT calculated absorption spectra (Figure

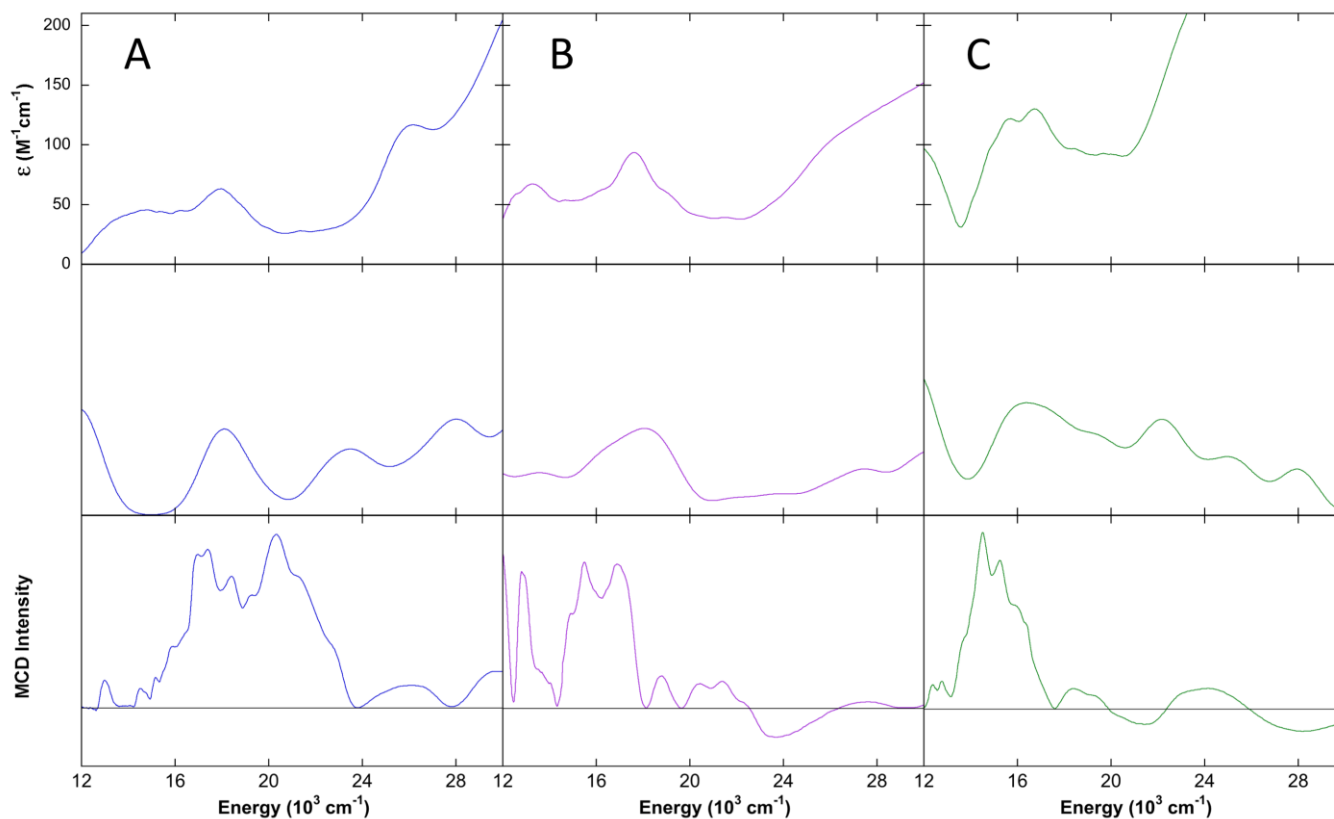


Figure 6: *Top:* 298 K Absorption spectra of for **1** (A, left, blue), **2** (B, middle, purple) and **3** (C, right, green). *Center:* Calculated Absorption Spectra for **1** (A, left, blue), **2** (B, middle, purple) and **3** (C, right, green). All spectra were red shifted 500 cm^{-1} for better comparison to experiment. *Bottom:* 5 K, 7 T UV-vis MCD spectra of **1** (A, left, blue), **2** (B, middle, purple) and **3** (C, right, green).

6, left, middle), the first transition, around 14000 cm^{-1} , has been assigned to two overlapping f-d transitions. This assignment to a metal-based transition was further supported by the increase in intensity in the MCD spectrum in this energy region as well as the somewhat decreased intensity when using EAS. The second transition, around 17500 cm^{-1} has been assigned to an $f-\pi^*$ transition. Transition three, centered around 27000 cm^{-1} has been assigned to a ligand p-f transition, while the fourth transition, around 30000 cm^{-1} has been assigned as a combination of ligand p-f and ligand p-d transitions. These same four broad transitions can also be fit to the MCD spectra, with slight changes in energy likely due to solvent distortions. By MCD, the first observed peak in the absorption spectra is shifted from 14000 cm^{-1} to 16500 cm^{-1} , the second from 17500 cm^{-1} to 20000 cm^{-1} . The third and fourth transitions do not change in energy significantly between the EAS and MCD spectra. Even with this shifts in energy, the assignments of these transitions as metal-based for transitions one and two, and ligand based for transitions three and four, are consistent with the intensity changes and line widths observed in these two techniques.

Similar observations can be made for complexes **2** and **3**. Based on the TDDFT calculated absorption spectra (Figure 6, center, middle), the first transition, around 14000 cm^{-1} , has been assigned to two overlapping f-d transitions. absorption spectra of complex **2** can also be assigned with at least 4 transitions across the energy region of 12000-30000 cm^{-1} (Figure 6, top, middle). The first transition, around 13000 cm^{-1} has been assigned as f-d in character. The second transition, centered around 17000 cm^{-1} , is made up of three separate transitions. The first is assigned to a combination of an f-d (78%) and $f-\pi^*$ (20%) transitions. The second and third are assigned to $f-\pi^*$

transitions. The third transition around 26000 cm^{-1} is assigned as two ligand p-f transitions, one with 71% contribution and the other 26%. The final transition is made up of three transitions, the first being an f-d transition, the second a mixture of ligand p-f (66%) and f-d (23%) character and the third a mixture of ligand p-d (75%) and ligand p-f (16%) character. Like complex **1** these transitions can be observed in the UV-vis MCD spectrum of **2**, with slightly shifted energies, where the assigned metal-based f-d transitions have increased intensity and the assigned CT transitions are weaker intensity, as expected.

For complex **3**, due to the large absorption feature in the high energy region, the transitions at lower energy are more difficult to observe so figure S7 has been included to highlight the agreement between experiment and theory for this complex. Based on the TDDFT calculated absorption spectra (Figure 6, left, middle), the first transition, around 14000 cm^{-1} , has been assigned to two overlapping f-d transitions (Figure 6, left, middle), the absorption spectrum can be assigned to at least 5 transitions across the energy region of 12000-30000 cm^{-1} (Figure 6, top right). The first, observed around 12000 cm^{-1} has been assigned to an $f-\pi^*$ transition and the second, around 15500 cm^{-1} is made up of two transitions, both $f-\pi^*$ in nature. The last three transitions are assigned to ligand p-d transitions. In this case, the MCD spectrum makes assignment of these transitions much clearer than in the EAS spectrum. In the EAS, these overlapping transitions result in a broad intense feature with very little insight into the number of transitions observed within that transition. In contrast, the MCD spectrum shows these three transitions as a series of negative, positive, negative bands across the 20000-30000 cm^{-1} energy region, allowing for the observation of the three-overlapping ligand p-d bands predicted by TD-DFT.

A description of the SO coupling and the multiconfigurational GSs is extremely important in the calculations of the magnetic properties. As seen here, however, the spectroscopic features in the UV-vis range, arising from the electrostatic and covalent interactions between the metal ion and the ligands, are well described by the scalar relativistic TD-DFT calculations. In the DFT ground state calculations, the U-ligand covalency is represented by a variety of 7s-, 6d-, and 5f- uranium and ligand orbital interactions. According to the NLMO analysis (Figure S5), each U-I orbital interaction in **1** is represented by a 2c-2e σ orbital and two 2c-2e π orbitals. However, the latter have only small U contributions. The σ bonding orbitals are also strongly polarized toward the ligands, but less so than the π orbitals. Each has 12% weight on uranium, involving mostly uranium 6d and 7s. Therefore, the U-I interactions in **1** are predominantly ionic, with some σ and weak π covalent contributions. There are multiple uranium orbital interactions with Tp* and THF ligand orbitals in **1**, with a total metal orbital weight of 8% on average in each U-N bonding orbital, representing N to U donation bonding, and smaller metal orbital weights in the U-O interactions. The analysis likewise shows that the U-I and U-N bonding features in complex **2** are very similar to complex **1**. Complex **3** shows 12% density weight at U in the U-C interaction (60% 6d; 26% 5f) and therefore more involvement of 5f compared to the U-I σ bonds of complex **1**. There are also six equivalent NLMO representing the U-N donation bonding interactions, analogous to those in complexes **1** and **2**. Overall, while each orbital representing partially covalent ligand-metal interactions is strongly polarized toward the metal, there are many of them, such that the U centers can be considered to be involved significantly in ligand-to-metal donation bonding. This conclusion is supported by the charges and valence electron configurations of the metal ion, as determined by the DFT NBO calculations, which are given in Table S3. The net charge at the U ion is 1.26, 1.37, and 1.71, for complex **1**, **2** and **3**, respectively. These values are considerably smaller than the formal charge of +3.

Experimental and Computational Studies of Tp*₂UBipy

In addition to the three U(III) complexes **1-3** highlighted thus far, an additional complex, **4**, was also investigated. Complex **4** has the same general Tp*U(ligand) structure, but instead of a simple halide or alkyl ligands it contains the redox non-innocent 2,2'-bipyridine (Bipy), resulting in the Tp*U(Bipy) complex. The Bipy ligand is one of the best-known redox-flexible ligands,⁴⁰ allowing for either one or two electrons in its π^* orbitals. Previously reported magnetic susceptibility studies performed at ambient temperature, as well as X-ray crystallographic data, supported formulation of **4** as a uranium(III) center with a redox-innocent bipyridine radical anion.²³ With this in mind, studies of compound **4** using EPR, EAS, and MCD spectroscopies were performed.

The 5 K EPR of solid complex **4** was obtained. If the electronic structure were U(III) with a redox innocent Bipy⁻ ligand, as previously suggested, one would expect to observe a spectrum consistent with complexes **1-3** with an additional transition around the spin-only value of $g = 2.0023$ for the Bipy⁻ ligand radical. Instead, the EPR of complex **4** showed no transitions. This suggests that, at 5 K, there is coupling of the unpaired electron of the U(III) center to the Bipy⁻ ligand resulting in a non-Kramers, EPR silent ground state for this complex. Further confirmation of this electronic structure came from the NIR MCD spectra. The 5 K, 7 T NIR MCD spectra of complex **4** (Figure 7) differs from that observed for complexes **1-3**. Instead of four groupings of very sharp signals followed by a fifth more broad series of transitions, which were observed for the trivalent

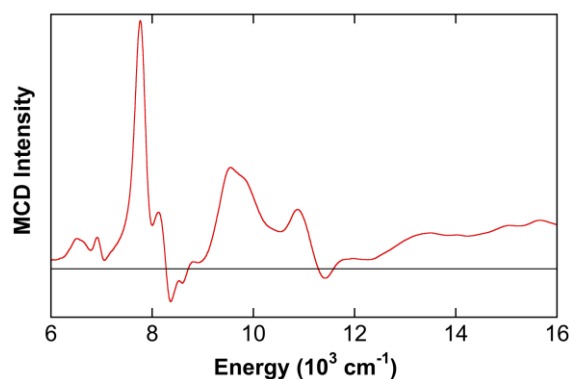


Figure 7: 5 K, 7 T NIR MCD spectrum of complex **4**.

complexes, the NIR MCD of complex **4** displays fewer sharp signals and overall, fewer spectral features. Experiments were performed as a function of magnetic field and temperature, demonstrating that all signals were consistent with a C-term mechanism (Figures S1/S2). While distinct from the trivalent complexes **1-3**, the NIR MCD of **4** appeared consistent with the general shape of the MCD for a series of non-Kramers uranium aryl complexes recently reported by our group.¹⁸ This commonality between the non-Kramers uranium(IV) aryl complexes and the uranium(III) complex **4** further suggested a coupling between the radical on the Bipy ligand and the uranium center.

In order to characterize the ground state of complex **4**, DFT/TD-DFT calculations were performed. Starting from a DFT calculation of the lowest-energy spin quintet, the ground state of **4** was identified by spin-flip TD-DFT to be a spin triplet. When the lowest spin triplet $M_s = 1$ component is calculated self-consistently, the unpaired electron in the Bipy⁻ ligand is represented by a β spin π orbital that shows weak overlap with the U center (Figure 8). The spin density evidences the antiferromagnetically coupled spin state, with the α spin density localized on uranium and the β spin density localized in the Bipy moiety. Inspection of the Kohn-Sham molecular orbitals for the triplet indicated the presence of ligand-metal donation bonding. The analysis revealed that there are six equivalent NLMOs corresponding to the U-N(Tp*) interactions, each possessing 7% weight on the metal center (52% 6d; 35% 5f). Furthermore, there are two equivalent orbitals showing σ interactions of the Bipy⁻ ligand (8% U weight, 9% 7s, 55% 6d and 36% 5f), and two equivalent π

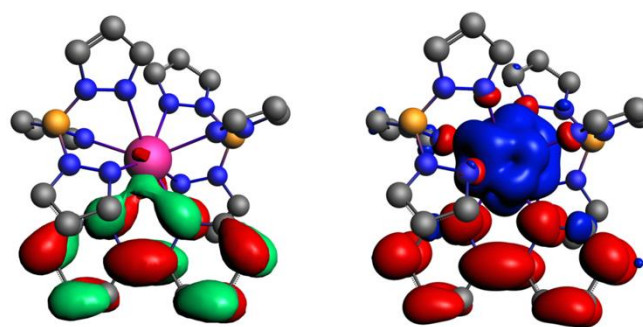


Figure 8: MO representing the unpaired electron in the 2,2'-bipyridine ligand (left) and spin density (right) for complex **4**. The isosurface values are ± 0.03 au and spin density isosurface are ± 0.001 au.

orbitals on the same ligand, strongly delocalized, as it is typical for aromatic systems, with 3% uranium weight each (33% 6d; 67% 5f).

To gain further insight into the interaction between the uranium center and the ligand environment, the 5 K, 7 T UV-vis MCD spectrum (Figure 9, bottom) was also obtained and all signals determined to be consistent with a *C*-term mechanism (Figures S1/S2) *vide supra*. The UV-vis MCD spectrum of **4** consists of several sharp transitions between 12000 and 18000 cm^{-1} followed by a broad pair of signals around 24000 cm^{-1} and 26000 cm^{-1} . Like complexes **1-3**, MCD (Figure 9, bottom) and electronic absorption (Figure 9, top, red solid) in the UV-vis region were obtained to gain insight into the metal-to-ligand and ligand-to-metal transitions which should be observed in this energy region. The absorption spectra were calculated to then assign the transitions of the experimental absorption spectra (Figure 9, top, black dashed). For these calculations, a functional with range-separated exchange was used due to the occurrence of charge-transfer states which led to an overall blue-shift of the calculated spectrum by about 5000 cm^{-1} , but otherwise good agreement regarding the overall appearance. Based on assignments of calculated absorption spectra, the spectrum consists of several broad transitions across the 12000-24000 cm^{-1} range followed by a single intense transition around 26000 cm^{-1} . Calculated absorption spectra were used to assign the experimentally observed transitions. The highest energy transitions observed around 26000 cm^{-1} was assigned to f-d transitions while the smaller transitions between 12000-24000 cm^{-1} are overlapping f-d and f- π^* transitions.

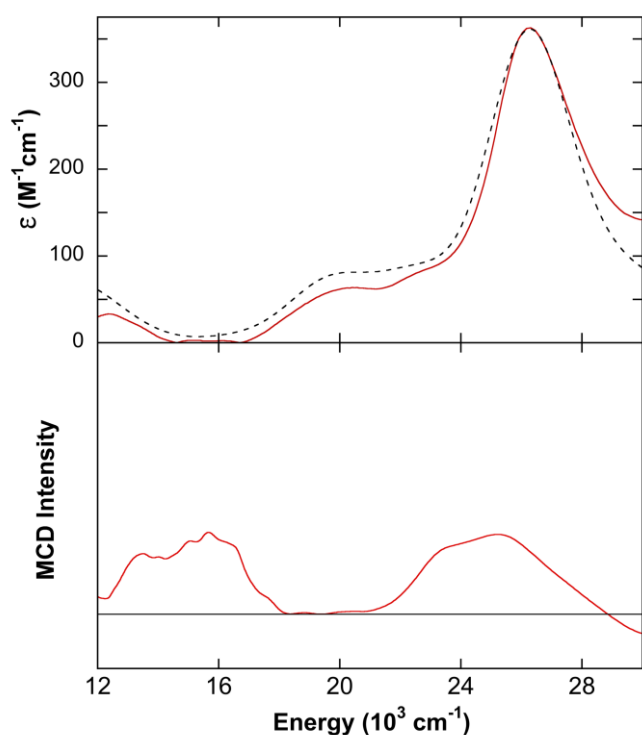


Figure 9: Electronic absorption spectrum (top, red solid), calculated absorption spectrum, red shifted 5000 cm^{-1} (top, black dashed), and 5 K, 7 T UV-vis (bottom) MCD spectrum of complex **4**.

Conclusions

Due to the novel reactivity of U(III) complexes, a fundamental understanding of the electronic structure and bonding is essential to build structure-functions relationships and develop new reactivity. However, the highly paramagnetic nature of these systems often makes spectroscopic insight difficult to obtain and interpret. We reported the use of electronic absorption, EPR, and MCD spectroscopies as well as DFT, TD-DFT, and multi-reference wavefunction calculations to evaluate the effect of ligand exchange on a series of uranium(III) Tp^* complexes.

Multi-reference wavefunction calculations provided electronic structure insight related to the EPR spectra. In all cases, the ground state was observed to have a large magnetic anisotropy. From these calculations it was also determined that the calculated spin and orbital angular momentum expectation values deviate strongly from the largest free ion projection quantum numbers. This results from the combined action of the strong spin-orbit coupling and the ligand field, and results in a sizable orbital angular momentum in these systems. The theoretically obtained *g*-factors are comparable to those observed experimentally.

This study also demonstrates the application of *C*-term MCD spectroscopy to U(III) complexes, a technique which has proven useful in evaluating oxidation states of uranium complexes and, when combined with detailed computational methods, detailed assignments of transitions. Overall, it was observed that, across complexes **1-3**, the ground state of the complexes remains unchanged and only minor perturbations were observed spectroscopically. The NIR MCD spectra of complexes **1-3** exhibit four groupings of very sharp, narrow transitions which were assigned as f-f transitions. The UV-vis MCD spectra exhibit a grouping of intense transitions followed by broader, less intense transitions. Due to the complexity of these systems, calculation of the MCD spectra were not feasible. Instead, TD-DFT calculations were used to assign the transitions observed in the UV-vis electronic absorption spectra.

The similarities in the observed transitions across the series of molecules suggests the ligand perturbation has a minimal effect on the electronic structure of the uranium(III) center, even when transitioning from a sigma/pi donor ligand like iodine to a strong sigma donor ligand like benzyl. While this lack of effect has been previously observed in a series of uranium(IV) aryl complexes,¹⁸ it differs significantly from what would be expected for ligand effects on the electronic structure of transition metal complexes containing metals such as iron. In these systems, slight ligand perturbations commonly result in pronounced changes in the electronic structure of the metal center, even to the extent of modifying the geometry and spin state of the complexes.⁴² Overall, this suggests that greater ligand perturbations are likely required to significantly modify reactivity in f-block systems compared to d-block systems.

Lastly, the combination of these experimental and theoretical techniques also redefined the ground state of a uranium(III) complex with a redox non-innocent ligand, identifying the presence of antiferromagnetic coupling between the U(III) center and the Bipy radical ligand of complex **4**. The lack of EPR signal suggested the assignment of U(III) with a magnetically un-coupled ligand radical was not appropriate at 5 K, and the 5 K NIR MCD spectrum displayed no sharp signals and overall, fewer spectral features than those observed for complexes **1-3**. This was further supported by DFT/TD-DFT calculations where the ground state was found to be a spin triplet, with an

antiferromagnetic coupled spin state between the uranium center and the Bipy ligand.

Overall, this study demonstrated the efficacy of the combined experimental MCD, EPR, and theoretical approach towards evaluating electronic structure and bonding in U(III) complexes, providing important insight into the challenges in altering ligand environments to modify bonding and reactivity in uranium coordination chemistry. Application of this approach to other uranium coordination complexes will continue to broaden our understanding of ligand contributions to bonding and reactivity in uranium coordination chemistry.

Conflicts of interest

The authors declare no conflicts of interest.

Acknowledgements

M.L.N acknowledges support for this work from the U.S. Department of Energy, Office of Science, Early career Research Program under Award DE-SC0016002. J.A. acknowledges support from the Center for Actinide Science and Technology, an Energy Frontier Research Center funded by the U.S. Department of Energy, Office of Science, Basic Energy Sciences, under Award Number DE-SC0016568. We thank the Center for Computational Research (CCR) at the University of Buffalo for providing computational resources. We would also like to acknowledge the Matson Lab for the use of their absorption instrument.

References

- H. H. Dam, D. N. Reinhoudt and W. Verboom, *Chem. Soc. Rev.*, 2007, **36**, 367-377.
- P. L. Arnold, *Chem. Commun.*, 2011, **47**, 9005-9010.
- B. M. Gardner and S. T. Liddle, *Eur. J. Inorg. Chem.*, 2013, **2013**, 3753-3770.
- M. A. Boreen, D. J. Lussier, B. A. Skeel, T. D. Lohrey, F. A. Watt, D. K. Shuh, J. R. Long, S. Hohloch and J. Arnold, *Inorg. Chem.*, 2019, **58**, 16629-16641.
- J. T. Coutinho, M. Perfetti, J. J. Baldoví, M. A. Antunes, P. P. Hallmen, H. Bamberger, I. Crassee, M. Orlita, M. Almeida, J. van Slageren and L. C. J. Pereira, *Chem. Eur. J.*, 2019, **25**, 1758-1766.
- S. Fortier, J. R. Aguilar-Calderón, B. Vlaisavljevich, A. J. Metta-Magaña, A. G. Goos and C. E. Botez, *Organometallics*, 2017, **36**, 4591-4599.
- S. M. Franke, B. L. Tran, F. W. Heinemann, W. Hieringer, D. J. Mindiola and K. Meyer, *Inorg. Chem.*, 2013, **52**, 10552-10558.
- C. Hennig, J. Tutschku, A. Rossberg, G. Bernhard and A. C. Scheinost, *Inorg. Chem.*, 2005, **44**, 6655-6661.
- B. Kosog, H. S. La Pierre, M. A. Denecke, F. W. Heinemann and K. Meyer, *Inorg. Chem.*, 2012, **51**, 7940-7944.
- S. T. Liddle, *Angew. Chem. Int. Ed.*, 2015, **54**, 8604-8641.
- L. Maria, I. C. Santos and I. Santos, *Dalton Trans.*, 2018, **47**, 10601-10612.
- J. Riedhammer, J. R. Aguilar-Calderón, M. Miehlich, D. P. Halter, D. Munz, F. W. Heinemann, S. Fortier, K. Meyer and D. J. Mindiola, *Inorg. Chem.*, 2020, **59**, 2443-2449.
- A.-C. Schmidt, A. V. Nizovtsev, A. Scheurer, F. W. Heinemann and K. Meyer, *Chem. Commun.*, 2012, **48**, 8634-8636.
- J. A. Seed, M. Gregson, F. Tuna, N. F. Chilton, A. J. Wooles, E. J. L. McInnes and S. T. Liddle, *Angew. Chem. Int. Ed.*, 2017, **56**, 11534-11538.
- C. J. Tatebe, S. A. Johnson, M. Zeller and S. C. Bart, *J. Organomet. Chem.*, 2018, **857**, 152-158.
- F. Gendron, V. E. Fleischauer, T. J. Duignan, B. L. Scott, M. W. Löble, S. K. Cary, S. A. Kozimor, H. Bolvin, M. L. Neidig and J. Autschbach, *Phys. Chem. Chem. Phys.*, 2017, **19**, 17300-17313.
- W. W. Lukens, N. M. Edelstein, N. Magnani, T. W. Hayton, S. Fortier and L. A. Seaman, *J. Am. Chem. Soc.*, 2013, **135**, 10742-10754.
- N. J. Wolford, D.-C. Sergentu, W. W. Brennessel, J. Autschbach and M. L. Neidig, *Angew. Chem. Int. Ed.*, 2019, **58**, 10266-10270.
- E. M. Matson, W. P. Forrest, P. E. Fanwick and S. C. Bart, *J. Am. Chem. Soc.*, 2011, **133**, 4948-4954.
- Y. Sun, R. McDonald, J. Takats, V. W. Day and T. A. Eberspacher, *Inorg. Chem.*, 1994, **33**, 4433-4434.
- M. A. Antunes, G. M. Ferrence, Â. Domingos, R. McDonald, C. J. Burns, J. Takats and N. Marques, *Inorg. Chem.*, 2004, **43**, 6640-6643.
- R. McDonald, Y. Sun, J. Takats, V. W. Day and T. A. Eberspacher, *J. Alloys Compd.*, 1994, **213-214**, 8-10.
- S. J. Kraft, P. E. Fanwick and S. C. Bart, *Inorg. Chem.*, 2010, **49**, 1103-1110.
- E. M. Matson, W. P. Forrest, P. E. Fanwick and S. C. Bart, *Organometallics*, 2013, **32**, 1484-1492.
- M. A. Boreen, T. D. Lohrey, G. Rao, R. D. Britt, L. Maron and J. Arnold, *J. Am. Chem. Soc.*, 2019, **141**, 5144-5148.
- A. Formanuk, A.-M. Ariciu, F. Ortu, R. Beekmeyer, A. Kerridge, F. Tuna, E. J. L. McInnes and D. P. Mills, *Nat. Chem.*, 2017, **9**, 578-583.
- J. Jung, S. T. Löffler, J. Langmann, F. W. Heinemann, E. Bill, G. Bistoni, W. Scherer, M. Atanasov, K. Meyer and F. Neese, *J. Am. Chem. Soc.*, 2020, **142**, 1864-1870.
- W. W. Lukens, M. Speldrich, P. Yang, T. J. Duignan, J. Autschbach and P. Kögerler, *Dalton Trans.*, 2016, **45**, 11508-11521.
- K. R. Meihaus, S. G. Minasian, W. W. Lukens, S. A. Kozimor, D. K. Shuh, T. Tylyszczak and J. R. Long, *J. Am. Chem. Soc.*, 2014, **136**, 6056-6068.
- F. Aquilante, J. Autschbach, A. Baiardi, S. Battaglia, V. A. Borin, L. F. Chibotaru, I. Conti, L. D. Vico, M. Delcey, I. F. Galván, N. Ferré, L. Freitag, M. Garavelli, X. Gong, S. Knecht, E. D. Larsson, R. Lindh, M. Lundberg, P. Å. Malmqvist, A. Nenov, J. Norell, M. Odellius, M. Olivucci, T. B. Pedersen, L. Pedraza-González, Q. M. Phung, K. Pierloot, M. Reiher, I. Schapiro, J. Segarra-Martí, F. Segatta, L. Seijo, S. Sen, D.-C. Sergentu, C. J. Stein, L. Ungur, M. Vacher, A. Valentini and V. Veryazov, *J. Chem. Phys.*, 2020, **152**, 214117.
- I. Fdez. Galván, M. Vacher, A. Alavi, C. Angeli, F. Aquilante, J. Autschbach, J. J. Bao, S. I. Bokarev, N. A. Bogdanov, R. K. Carlson, L. F. Chibotaru, J. Creutzberg, N. Dattani, M. G. Delcey, S. S. Dong, A. Dreuw, L. Freitag, L. M. Frutos, L. Gagliardi, F. Gendron, A. Giussani, L. González, G. Grell, M. Guo, C. E. Hoyer, M. Johansson, S. Keller, S. Knecht, G. Kovačević, E. Källman, G. Li Manni, M. Lundberg, Y. Ma, S. Mai, J. P. Malhado, P. Å. Malmqvist, P. Marquetand, S. A. Mewes, J. Norell, M. Olivucci, M. Oettel, Q. M. Phung, K. Pierloot, F. Plasser, M. Reiher, A. M. Sand, I. Schapiro, P. Sharma, C. J. Stein, L. K. Sørensen, D. G. Truhlar, M. Ugandi, L. Ungur, A. Valentini, S. Vancoillie, V. Veryazov, O. Weser, T. A. Wesolowski, P.-O. Widmark, S. Wouters, A. Zech, J. P. Zobel and R. Lindh, *J. Chem. Theory Comput.*, 2019, **15**, 5925-5964.

32. J. Autschbach, *Comment. Inorg. Chem.*, 2016, **36**, 215-244.
33. F. Gendron, H. Bolvin and J. Autschbach, in *Organometallic Magnets*, eds. V. Chandrasekhar and F. Pointillart, Springer International Publishing, Cham, 2019, DOI: 10.1007/3418_2018_6, pp. 355-390.
34. F. Gendron, D. Páez-Hernández, F.-P. Notter, B. Pritchard, H. Bolvin and J. Autschbach, *Chem. Eur. J.*, 2014, **20**, 7994-8011.
35. F. Gendron, B. Pritchard, H. Bolvin and J. Autschbach, *Dalton Trans.*, 2015, **44**, 19886-19900.
36. M. Karbowiak, Z. Gajek and J. Drożdżyński, *Chem. Phys.*, 2000, **261**, 301-315.
37. E. D. Glendening, C. R. Landis and F. Weinhold, *WIREs Computational Molecular Science*, 2012, **2**, 1-42.
38. E. D. Glendening, C. R. Landis and F. Weinhold, *J. Comp. Chem.*, 2013, **34**, 1429-1437.
39. R. L. Martin, *J. Chem. Phys* 2003, **118**, 4775-4777.
40. C. Kaes, A. Katz and M. W. Hosseini, *Chem. Rev.*, 2000, **100**, 3553-3590.
41. M. Halcrow, *Crystals*, 2016, **6**, 58.

Ligand Effects on Electronic Structure and Bonding in U(III) Coordination Complexes: A Combined MCD, EPR and Computational Study

Nikki J. Wolford, Xiaojuan Yu, Suzanne C. Bart, Jochen Autschbach, Michael L. Neidig

Spectroscopy and theory enable broader insight into electronic structure and bonding in U(III) coordination complexes, focusing on systems with Tp* ligands.

